Proceedings of the
Annual Stability Conference
Structural Stability Research Council
Grapevine, Texas, April 17-20, 2012

Flexural Strength of Exterior Metal Building Wall Assemblies with Rigid Insulation

T. Gao[1], C.D. Moen[2], P. Mueller[3]

Abstract

The critical load case for cold-formed steel girts in a metal building wall system is suction caused by wind loading. In North America, the girt flexural capacity for this load case is predicted with experimentally derived strength reduction factors, i.e., R-factors in AISI S100. This paper presents 50 vacuum box tests to determine the R-factors for the wall system with the rigid board insulation sandwiched between girts and panels. The testing variables include girts cross-section, panel type, insulation thickness and fastener. Different failure modes are observed in the test series, and the wall system capacity is influenced by the failure mode. The R-factors for the wall system with the rigid board insulation is presented.

1. Introduction

The critical load case for cold-formed steel wall girts in a metal building wall system is suction caused by wind. As wind pulls the wall away from the building, the girt unbraced flanges are placed in compression, resulting in lateral-torsional buckling deformation. Girt rotation is amplified in a C-section by torsion-induced shear flow caused by the load eccentricity from fastener line to the C-section shear center (Trahair 1993) as shown in Fig. 1a, and for a Z-section by biaxial bending about the inclined principal axes as shown in Fig. 1b (Zetlin and Winter 1955, Thomasson 1988, Murry 1985).

[1]Graduate Research Assistant, Virginia Tech, <gaot@vt.edu>
[2]Assistant Professor, Virginia Tech, <cmoen@vt.edu>
[3]Undergraduate Researcher, Virginia Tech, <paulm17@vt.edu>

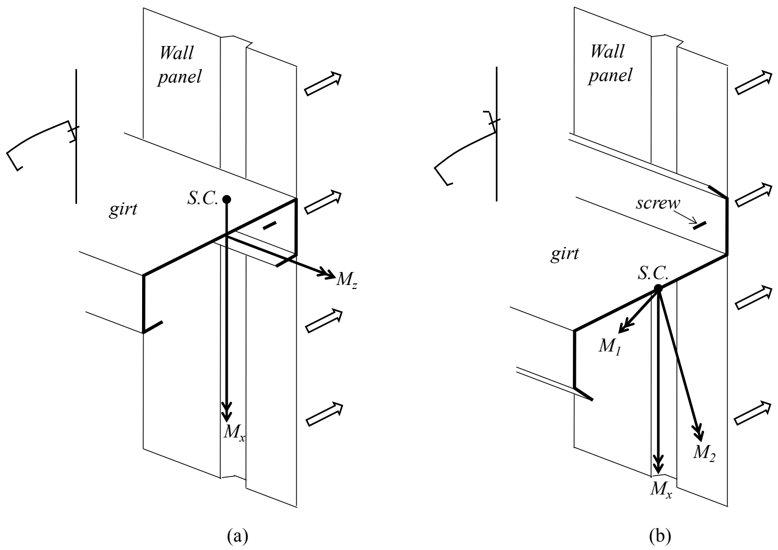

Figure 1: Girts rotation due to (a) torsion in a C-section from the load eccentricity, and (b) biaxial bending in a Z-section

The amount of rotational restraint provided by the through-fastened connection to the metal wall panel as the girt rotates defines girt flexural capacity (LaBoube 1986, Rousch and Hancock 1996, Gao and Moen 2012a and 2012b). In North America, the influence of rotational restraint on girt flexural capacity, M_n, is predicted for the wind suction case with experimentally derived strength reduction factors, i.e., R-factors, as described in AISI S100-07 D6.1.1 (AISI 2007), where $M_n=RF_yS_e$ and S_e is the effective section modulus of the girt about its strong centroidal axis including local buckling. In Europe (EN-1993 2006) and Australia (AS/NZS-4600 2005), the free compressed flange is treated as a column on an elastic foundation (Peköz and Soroushian 1982), where the foundation spring, representing the rotational restraint provided by the web and through-fastened connection, is calculated with experiments (LaBoube 1986, Rousch and Hancock 1996) or empirical equations (EN-1993 2006).

The worldwide sustainability movement is motivating design and construction code changes that emphasize energy efficiency (e.g., ASHRAE-90.1 2010). To meet these stringent energy standards, the metal building industry is exploring alternative insulation materials to fiberglass blanket. One option for providing a continuous thermal barrier is rigid board insulation, typically a polyisocyanurate foam with trilinear stress-strain properties in compression. The insulation board is manufactured in different thicknesses, most commonly 25.4 mm and 50.8 mm, and has been installed in thicknesses as high as 101.6 mm (MBMA 2009).

Rotational restraint studies with rigid board insulation through-fastened between a girt and metal panel have shown that rotational restraint increases as a function of rigid board insulation thickness (Gao and Moen 2012b). The insulation acts as a washer against the metal panel, spreading the fastener force and reducing local deformation in the metal panel (Fig. 2a). Rotational stiffness is also influenced by the compressive stress-strain properties of the rigid board insulation because as the girt tends to rotate under load, the pivot point on the flange indents the insulation. Rotational restraint was shown to mimic the insulation trilinear compressive stress-strain curve (Fig. 2b) – initially very stiff until the cell walls of the foam buckled, then a region of lower stiffness as the air voids in the insulation are compressed, and then increased stiffness because of the higher material density.

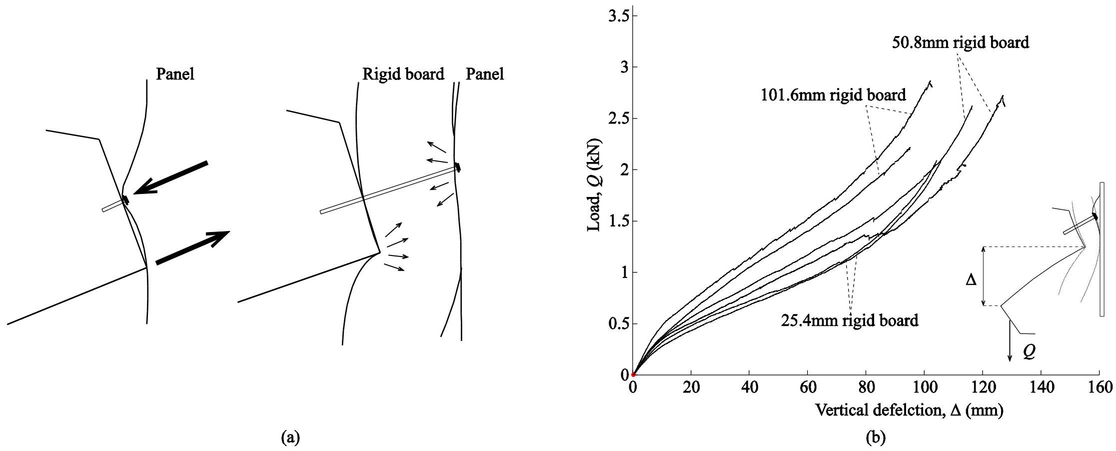

Figure 2: Rigid board influences girt rotational restraint: (a) fastener force spreads out across panel, and (b) girt rotational restraint is trilinear (Gao and Moen 2012b)

The goal of the research study summarized herein was to experimentally observe and quantify the influence of rigid board insulation on through-fastened girt capacity. The test program studied rigid board insulation thickness (25.4 mm, 50.8 mm, 2 x 50.8 mm) and type (e.g., Thermax and XPS) with vacuum box tests. The experimental details, strength comparisons and failure modes are discussed and documented in the following sections.

2. Experimental Program

2.1 Test setup

The test setup is designed to mimic exterior wind suction that pulls a wall outward and away from a metal building, placing the free girt flanges in compression. Each wall specimen is constructed with two simple span parallel girts with their free flanges facing up in the box. The girts with a centerline bearing span of 7468 mm (Fig. 4b) are through-fastened to a wall panel (4140 mm wide) at a spacing of 2286 mm as shown in Fig. 4a. The pressure box is sealed with plastic sheeting from above and air is pulled out below the specimen with vacuum pumps to simulate the suction loading.

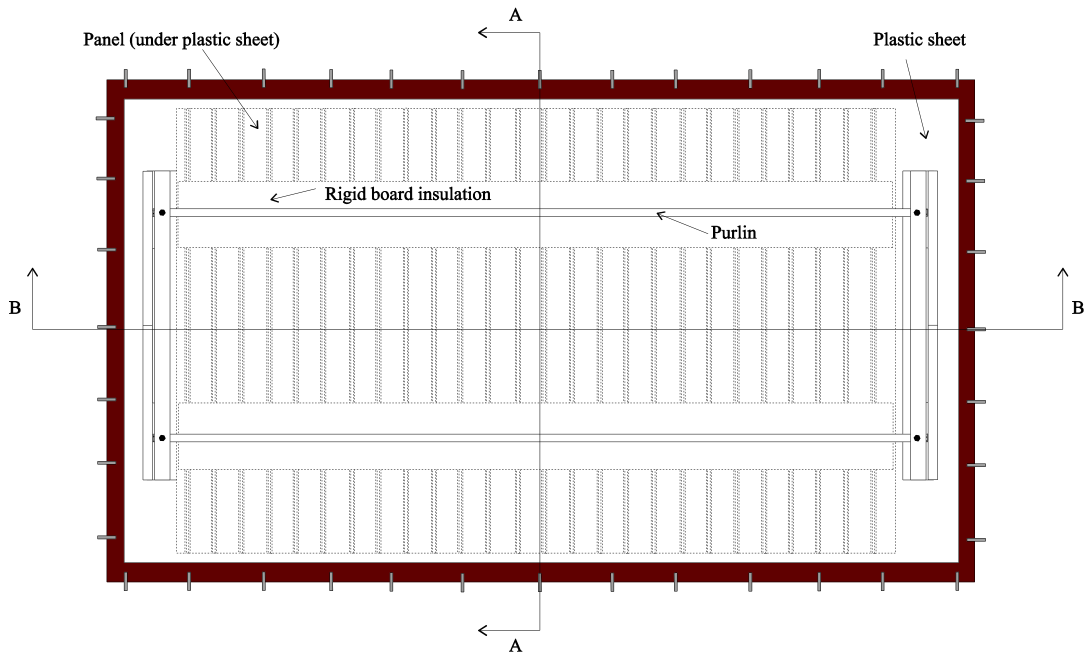

Figure 3: Test setup plan

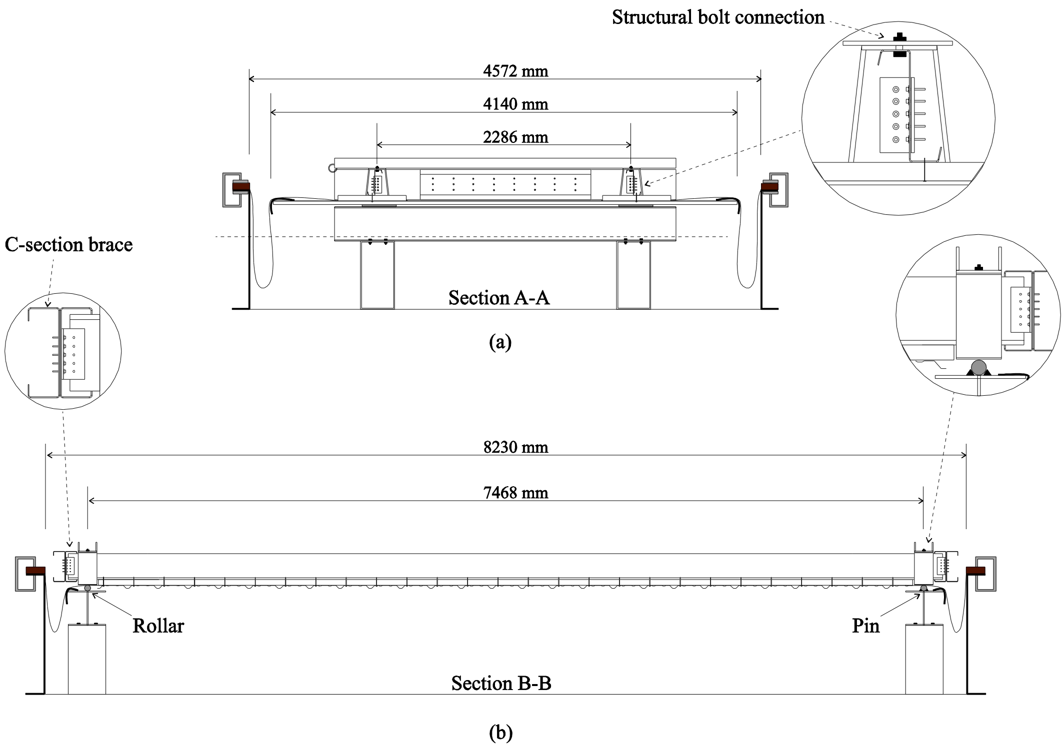

Figure 4: Test setup (a) section A-A (b) section B-B in Fig. 3

2.2 Test matrix

A total of 50 pressure box experiments were performed and the test matrix is shown in Table 1. The specimen naming convention is: girt profile (C- or Z-section), approximate web depth, metal panel type (Durarib or Bigbee), insulation type (R: fiberglass blanket; TH: Thermax), approximate insulation thickness, specimen number within a specific series (1 or 2) and fastener with a washer (W). The girt cross-section dimensions were selected to explore the dimensional limits specified in the North American R-factor strength prediction approach (AISI 2007, Section D6.1.1) summarized in Table 1, i.e., partially effective (locally slender) and fully effective (locally stocky) C- and Z-sections were chosen.

Dow Thermax rigid board insulation was the focus of this study (Tests 16-50 in Table 1), although bare panel tests (Tests 1-13 in Table 1) and tests with R13 fiberglass blanket insulation (Tests 14-15 in Table 1) were also performed to provide a baseline (control) for evaluating the influence of rigid board on wall girt capacity. The bare panel and R13 tests also accommodated a comparison between this test setup and existing data that was used to define the current AISI R-factors (Fisher 1996). The R13 fiberglass insulation uncompressed thickness was 101.6 mm. The influence of rigid board insulation thickness was evaluated with tests employing 1- 25.4 mm insulation sheet, 1- 50.8 mm sheet, and 2 - 50.8 mm (101.6 mm total) sheets.

Metal panel profile, thickness, and stress-strain properties have all been shown to influence rotational restraint (LaBoube 1986, Gao and Moen 2012a). In this study, two 26 gauge (0.46mm thick) panels types (NCI Durarib and Bigbee), were used with dimensions shown in Fig. 5. The 26 gauge panel was selected because this is the minimum allowable thickness specified in the North American specification for the R-factor method (AISI 2007 Section D6.1.1) The yield stress for each panel type was measured with a tensile tests (ASTM E8M 2000), with the Durarib panel having 380 MPa yield stress and a ductile failure at 22% engineering strain and the Bigbee panel having 620 MPa yield stress and a more brittle failure strain.

Two sizes of screws without washers were used to fasten the panel to the girts: 127 mm #1/4-14 self-drilling screws were used for the test specimens with the thickest rigid board insulation (101.6 mm, see "TH100" in Table 1) and #12 screws for all other test specimens. The diameters of #1/4-14 and #12 screws were measured to be 5.36 mm and 4.62 mm, respectively. In Test 5 only (Z-girts, panel-B, no insulation) #12 screws with washers were used.

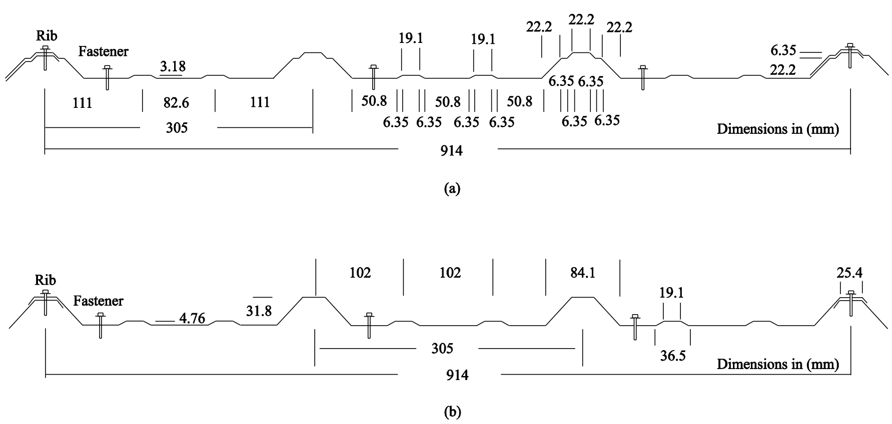

Figure 5: Cross-section of (a) panel-D and (b) panel-B and fastener location

2.3 Test boundary conditions

The support boundary conditions were implemented as roller and pin as shown in Fig.4. A transverse screw-fastened C-section brace was installed before each test to provide a rigid torsional restraint at the girt supports (Fig. 4). The advantages of this test setup are that the influence of catenary action (i.e., tension stiffening) is eliminated and the girt moment distribution (parabolic) and moment magnitude ($wL^2/8$) are known, making comparisons of tested strength to strength predictions more straightforward. The disadvantage of this test setup is that it is not representative of the true boundary conditions in a metal building.

2.4 Specimen construction

Each wall specimen was constructed with a special jig that held the two girts in place while the metal panels were through-fastened to the girts at a 305 mm spacing. The specimens were constructed with the panel facing up to accommodate fastener placement, and then the wall was flipped over with an overhead crane and placed in the pressure box, see (Gao and Moen 2011) for details. The screws fastening the panel to the girts were installed adjacent to the rib consistent with industry practice, and the screws lapping the panel were installed at the middle of the rib (see Fig. 5).

Preliminary tests demonstrated that the 26 gauge metal panels failed before the girts because the tested boundary conditions for the panels are not continuous in bending, causing large moments at the transverse midspan. To prevent the panel flexural failure, the panels were stiffened with 1524 mm wide 26 gauge panel strips at midspan. Since girt spacing (2286 mm) is wider than the panel strips, the flange was through fastened to a single panel, and therefore it is assumed that the reinforcement did not interfere with the connection zone. Rigid board insulation strips wide were fixed to the girt flanges with self-drilling screws, and then the metal panels were through-fastened to the girt flanges. The insulation was sandwiched between the panels and flanges. Although the flange centerlines were approximately marked on the panels, it was still difficult to install the screws at the center of the flange due to the rigid board thickness. The screw locations on the flange were measured after each test and are summarized in the following section.

2.5 Specimen measurements and material properties

The measured out-to-out dimensions and base metal thickness for the failed girts are provided in Table 1. Girt sweep was measured at midspan on the free flange by running a stringline. The yield stress was measured with a tensile test from the flanges and web of failed girt (ASTM E8M 2000), the average of which is provided in Table1.

Table 1: Specimen dimensions, sweep imperfections and yield stress

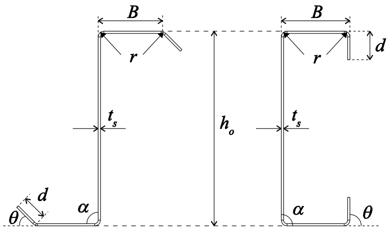

#	Test name	Cross-section											Girt imperfection at midspan	Yield stress
		Compression				Tension								
		B	d	α	θ	B	d	α	θ	h_o	r	t_s		
		mm	mm	deg.	deg.	mm	mm	deg.	deg.	mm	mm	mm	mm	MPa
1	Z200D-1	-	-	-	-	-	-	-	-	-	-	-	-	-
2	Z200D-2	68.4	26.4	92	47	72.5	27.5	92	53	202	6.55	2.59	-	420
3	Z200D-3	68.1	25.2	91	47	65.5	25.7	90	53	204	8.18	2.54	-	415
4	Z200B-1	68.6	24.4	90	47	70.1	28.0	90	52	205	7.27	2.57	-	433
5	Z200B-2W	68.0	25.8	91	46	70.1	26.1	91	53	204	6.68	2.57	0.25	418
6	Z250D-1	72.0	19.8	90	55	73.3	20.3	91	46	253	7.00	1.52	0.08	403
7	Z250D-2	72.0	20.8	90	55	72.6	21.4	90	48	253	6.47	1.52	1.83	401
8	Z250B-1	71.7	21.1	91	55	72.9	22.1	90	47	253	5.86	1.51	-0.28	401
9	Z250B-2	70.7	22.3	91	54	73.3	20.3	91	47	251	6.10	1.50	-3.12	399
10	C200D-1	65.2	21.3	92	90	65.0	21.7	92	90	203	5.11	2.57	-13.0	522
11	C200D-2	65.8	21.3	88	90	64.5	21.3	88	90	203	5.84	2.57	-8.31	519
12	C250D-1	64.5	20.9	90	89	65.5	19.6	90	89	254	5.61	1.49	0.28	423
13	C250D-2	63.8	20.8	89	91	65.0	19.3	89	91	254	5.51	1.50	-2.97	414
14	Z200D-R100-1	67.9	25.2	90	48	67.9	27.6	90	53	205	5.66	2.54	-	428
15	Z200D-R100-2	67.9	25.6	90	47	67.9	26.5	90	52	205	6.31	2.51	-	418
16	Z200D-TH25-1	70.6	25.3	92	46	70.8	28.0	91	52	204	7.14	2.54	-	428
17	Z200D-TH25-2	66.1	26.3	90	47	69.4	26.3	89	53	205	6.25	2.54	-	418
18	Z200D-TH50-1	73.3	24.1	91	48	69.3	26.2	90	53	202	7.74	2.57	-	423
19	Z200D-TH50-2	68.8	26.1	91	47	66.8	21.3	91	52	201	10.5	2.57	-	426
20	Z200D-TH100-1	69.7	22.6	92	47	70.1	26.7	90	53	201	7.62	2.57	-	427
21	Z200D-TH100-2	69.6	25.2	90	46	70.8	28.5	90	54	203	6.90	2.59	-	421
22	Z200B-TH25-1	70.0	26.2	90	46	70.3	27.8	88	53	204	6.08	2.54	-	421
23	Z200B-TH25-2	68.9	26.6	91	46	68.1	26.7	91	53	204	6.50	2.54	-	420
24	Z200B-TH50-1	72.1	25.1	89	48	71.4	28.0	89	53	203	7.52	2.57	-	424
25	Z200B-TH50-2	68.0	25.2	90	47	68.7	26.8	90	53	206	7.75	2.57	-	424
26	Z200B-TH100-1	68.1	26.0	90	47	68.7	25.0	90	52	202	6.74	2.57	-5.44	421
27	Z250D-TH25-1	68.4	20.1	92	54	73.9	20.8	91	47	253	6.46	1.50	-	404
28	Z250D-TH25-2	67.7	18.7	91	55	72.6	20.2	90	47	254	5.56	1.50	-	409
29	Z250D-TH50-1	67.2	21.1	90	54	71.9	20.7	91	47	252	6.49	1.54	-3.89	405
30	Z250D-TH50-2	71.9	20.1	91	56	72.9	20.6	91	47	253	6.32	1.54	2.87	402
31	Z250D-TH100-1	71.9	21.9	91	55	71.6	19.9	90	48	257	6.92	1.52	2.06	397
32	Z250D-TH100-2	72.0	22.0	90	54	73.0	20.0	90	46	253	6.07	1.52	8.28	409
33	Z250B-TH25-1	74.7	22.0	91	55	70.2	21.5	91	47	254	5.99	1.50	5.44	402
34	Z250B-TH25-2	69.3	20.4	90	55	72.5	20.1	89	47	258	6.25	1.52	1.55	398
35	Z250B-TH50-1	69.4	19.1	90	55	71.2	20.5	90	48	253	5.91	1.52	0.08	398
36	Z250B-TH50-2	68.0	19.4	90	55	70.0	19.8	90	48	254	5.66	1.52	3.86	402
37	Z250B-TH100-1	68.0	18.0	90	53	72.9	20.0	88	45	254	5.14	1.52	6.38	388
38	Z250B-TH100-2	68.1	22.6	90	54	72.8	20.2	88	47	254	6.80	1.52	2.92	409
39	C200D-TH25-1	63.8	21.0	93	90	64.5	21.0	93	90	203	4.81	2.57	-10.1	525
40	C200D-TH25-2	66.8	20.3	92	90	64.4	20.9	92	90	203	4.60	2.57	-12.8	526
41	C200D-TH50-1	61.5	21.2	91	90	62.8	20.2	91	90	203	3.96	2.58	-12.5	514
42	C200D-TH50-2	62.3	20.1	88	90	68.0	21.7	88	90	203	5.80	2.57	-8.31	531
43	C200D-TH100-1	64.7	21.2	87	90	65.7	21.0	87	90	203	6.34	2.57	-10.4	541
44	C200D-TH100-2	64.4	21.3	88	91	64.9	21.1	88	91	203	4.65	2.57	-7.92	547
45	C250D-TH25-1	63.1	21.2	89	90	63.2	20.9	89	90	254	4.34	1.49	-5.18	411
46	C250D-TH25-2	62.9	20.9	89	89	64.4	20.3	89	89	254	4.29	1.50	-3.40	410
47	C250D-TH50-1	63.1	20.1	90	90	68.1	21.3	90	90	254	4.85	1.50	-0.30	413
48	C250D-TH50-2	63.1	21.1	90	90	68.8	19.0	90	90	254	5.56	1.50	0.25	413
49	C250D-TH100-1	64.1	19.7	90	89	65.2	18.9	90	89	254	4.41	1.50	1.93	417
50	C250D-TH100-2	62.7	20.7	90	91	65.0	18.0	90	91	254	4.76	1.50	2.59	413

Name convention: girt profile, web depth, panel type, - ,insulation type, insulation thickness, - ,series number, washer
#1/4-14 self-drulling screws for "TH100" tests; #12 self-drilling screws for all other tests

2.6 Instrumentation

A Vishay Micro-Measurements Model 5100B data acquisition system was used to digitally record six data channels at 10 points per second. Two pressure transducers with an accuracy of ±15 Pa were used to measure the pressure inside the vacuum box. The transducers were calibrated with a water tube manometer with a procedure documented in (Gao and Moen 2009). Four wire potentiometers with an accuracy of ±0.4 mm were mounted to an angle resting on the girt free flanges and measured the vertical and lateral displacement of the free flange relative to a fixed datum as shown in Fig. 6. Video cameras recorded girt deformation during each test, see Moen (2012) to watch the videos.

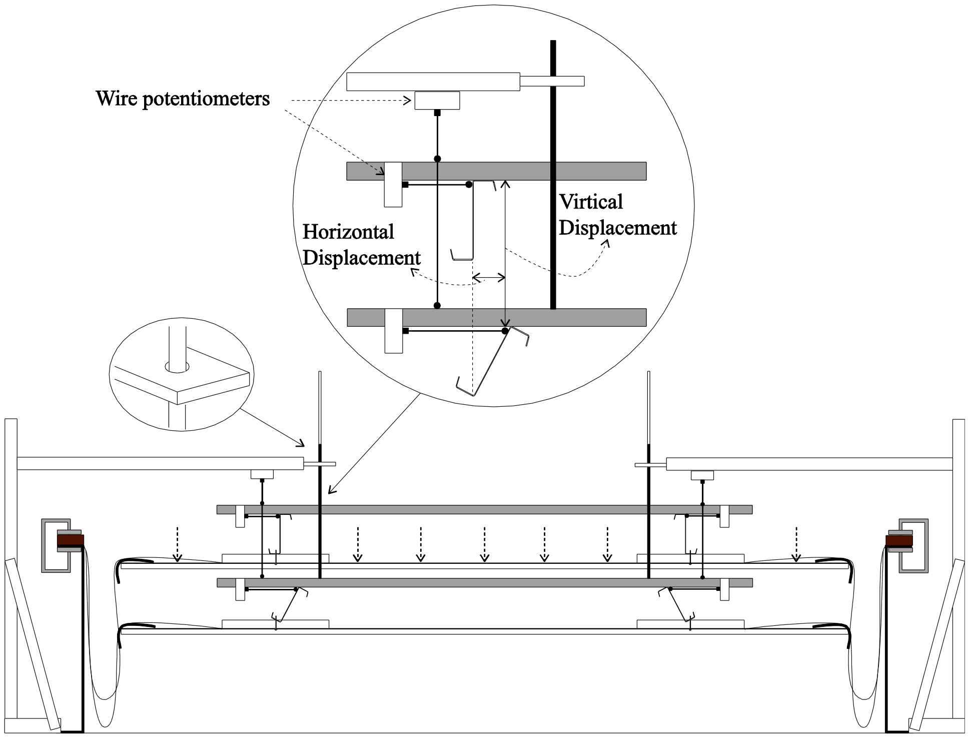

Figure 6: Instrumentation

2.7 Test procedure

Before recording data, the vacuum pump was turned on with all vents open for one minute to zero the pressure. Immediately after data and video collection began, two supplemental vacuums were turned on, followed by the manual closing of the vents until specimen failure. The loading rate could not be finely controlled; however, the loading rate was approximately 10 Pa/sec.

3. Test Results

3.1 Flexural capacity

The R-factor is calculated as:

$$R = \frac{M_t}{S_e F_y} \times 10^6 \tag{1}$$

where S_e is the effective section modulus which was calculated with the commercial software CFS (RSG 2007) based on the girt dimensions shown in Table 1; F_y is the yield stress shown in Table 1; M_t is the failure moment calculated as:

$$D\,(\text{N/m}) = \frac{PL_p}{1000} + \frac{1000d_p}{w} + \frac{1000d_g}{L_g} \tag{2}$$

$$M_t\,(\text{kN - m}) = \frac{P\times(L_g/1000)^2}{8}/1000 \tag{3}$$

where the panel length, L_p=4140 mm; the girt span, L_g=7468 mm; the weight of a single metal panel d_p=156N; the girt weight, d_g=525N (Z200), 356N (Z250), 507N (C200), 347N(C250); and a single metal panel width, w=914mm. The maximum pressure, P, S_e, M_t, R-factor and c are summarized in Table 2.

It has been shown by Gao and Moen 2012a and 2012b that the rotational restraint provided to the girt is dependent on the screw location c, which is the distance between the girt bearing pivot point and the center of the screw hole (see Fig. 7). Since the girt capacity was expected to be sensitive to the value of c, it was measured after each test. Specifically, the distance between the pivot point and the screw hole edge, e, was measured with a digital caliper (Fig. 7) on failed girts over the middle half of the span. Screw location, c, is the average e plus half of the screw's diameter, d/2, as shown in Fig. 7.

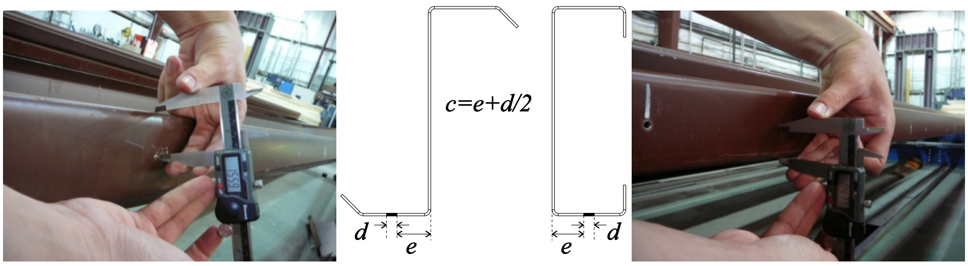

Figure 7: Screw location c measurement

Table 2: Flexural capacity and R-factors

#	Test name	P (Pa)	S_e (mm^3)	M_t (kN-m)	R	c (mm)
1	Z200D-1	-	-	-	-	-
2	Z200D-2	786	58562	11.93	0.48	39
3	Z200D-3	757	57353	11.52	0.48	37
4	Z200B-1	865	56922	13.08	0.53	41
5	Z200B-2W	893	58259	13.48	0.55	36
6	Z250D-1	461	35832	7.09	0.49	35
7	Z250D-2	454	36256	6.98	0.48	31
8	Z250B-1	440	36107	6.78	0.47	25
9	Z250B-2	478	36725	7.33	0.50	42
10	C200D-1	797	51016	12.10	0.45	34
11	C200D-2	692	50987	10.58	0.40	26
12	C250D-1	330	33743	5.19	0.36	20
13	C250D-2	330	33956	5.19	0.37	28
14	Z200D-R100-1	807	57584	12.24	0.50	40
15	Z200D-R100-2	473	58107	7.42	0.31	21
16	Z200D-TH25-1	770	57273	11.70	0.48	37
17	Z200D-TH25-2	818	58816	12.39	0.50	45
18	Z200D-TH50-1	849	55552	12.85	0.55	37
19	Z200D-TH50-2	802	55105	12.16	0.52	36
20	Z200D-TH100-1	722	54359	11.01	0.48	28
21	Z200D-TH100-2	961	57266	14.46	0.60	53
22	Z200B-TH25-1	865	58338	13.08	0.53	42
23	Z200B-TH25-2	654	58774	10.03	0.41	32
24	Z200B-TH50-1	1008	57119	15.14	0.63	47
25	Z200B-TH50-2	913	58071	13.77	0.56	40
26	Z200B-TH100-1	850	57469	12.86	0.53	34
27	Z250D-TH25-1	468	35396	7.19	0.50	39
28	Z250D-TH25-2	463	34662	7.12	0.50	36
29	Z250D-TH50-1	430	35663	6.64	0.46	28
30	Z250D-TH50-2	463	35722	7.12	0.50	30
31	Z250D-TH100-1	559	37707	8.50	0.57	44
32	Z250D-TH100-2	425	36615	6.57	0.44	31
33	Z250B-TH25-1	411	37279	6.36	0.42	27
34	Z250B-TH25-2	525	36522	8.02	0.55	39
35	Z250B-TH50-1	559	34757	8.50	0.61	41
36	Z250B-TH50-2	525	34932	8.02	0.57	39
37	Z250B-TH100-1	511	34156	7.81	0.59	37
38	Z250B-TH100-2	540	37186	8.22	0.54	40
39	C200D-TH25-1	464	50895	7.28	0.27	20
40	C200D-TH25-2	511	49774	7.97	0.30	26
41	C200D-TH50-1	559	50938	8.66	0.33	21
42	C200D-TH50-2	654	50377	10.03	0.38	24
43	C200D-TH100-1	821	50471	12.44	0.46	26
44	C200D-TH100-2	535	50348	8.31	0.30	12
45	C250D-TH25-1	287	34308	4.57	0.32	22
46	C250D-TH25-2	378	34133	5.88	0.42	33
47	C250D-TH50-1	301	33348	4.78	0.35	22
48	C250D-TH50-2	215	34149	3.54	0.25	12
49	C250D-TH100-1	320	33199	5.06	0.37	22
50	C250D-TH100-2	420	33998	6.50	0.46	30

4. Failure modes and influence of experimental variables

4.1 Effect of Screw Location

During the study, it was found that the girt capacity is very sensitive to the screw location *c*. For example, in Fig. 8, when *c* decreased from 53mm to 28mm for the same specimen type (Z200, panel-D, 101.6mm Thermax) the maximum pressure at failure decreased by 30%. Also, larger girt rotation was observed in the test with *c*=28mm. To remove the influence of *c* in the comparison of each result, a correction method will be proposed in section 4.3.

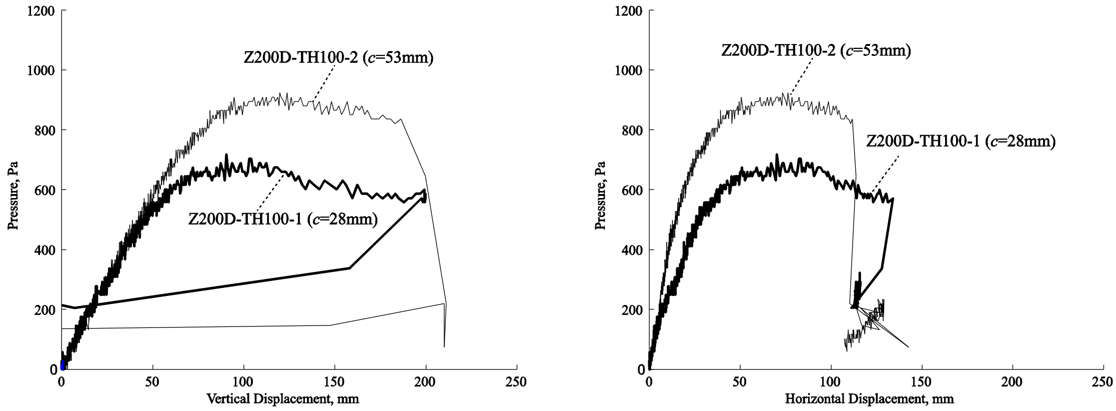

Figure 8: Effect of screw location c on the girt load-deformation response (a) vertical displacement (b) horizontal displacement (see Fig. 6 for vertical and horizontal displacement measurement)

4.2 Failure Modes

Z-section girts (203 mm deep, 2.54mm thick)

The common failure mode for Z-section girt specimens with locally stocky, rigid cross-sections was panel pull-over (Mode 2 in Table 3). In the case of bare panel (both panel-D and B) and fiberglass insulation, the panel suddenly pulled over the screw heads due to the girt rotation. As shown in Fig. 9, there is little permanent deformation in the girts.

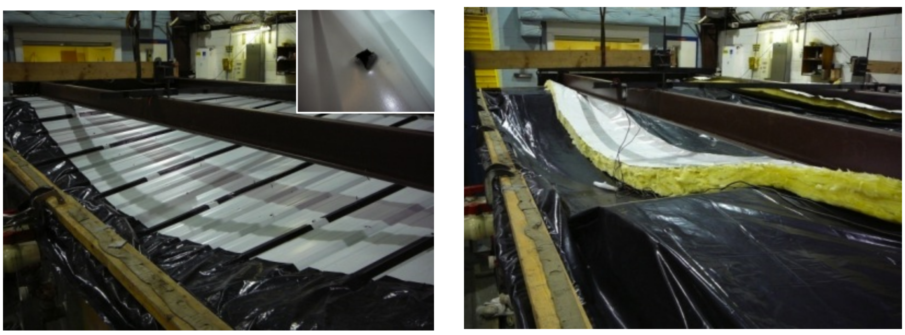

Figure 9: Panel pull-over failure in the bare panel tests

When the rigid board insulation was added, the failure mode changed to a combination of panel pull-over, bent and/or broken screws, and girt yielding as shown in Fig. 10. Screw bending was initiated by the presence of rigid board insulation as illustrated in Fig. 11 because of the distance (board thickness) between the girt flange and panel, which allowed the girt to rotate, creating a concentrated moment on the fasteners.

Figure 10: Failure mode in the test with 25.4 mm of rigid board

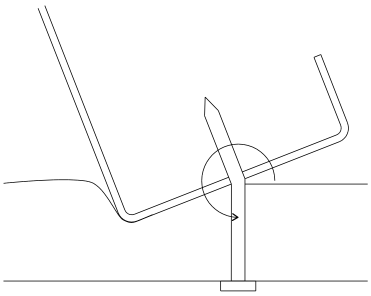

Figure 11: Screw bending due to existing of rigid board

When Z200 specimens with 50.8mm rigid board insulation were tested, the failure mode was a combination of screw bending/fracture and girt yielding. Panel pull-over was prevented by the rigid board insulation's "washer effect" which reinforced the panel and prevented local panel deformation. For a rigid board thickness of 101.6mm, the only failure mode observed was girt yielding. Screw bending was not observed because of the larger screw diameter employed (#14-1/4).

Z-girts (254mm deep, 1.52mm thick)

All Z250 (bare panel and rigid board insulation) girts failed by girt local buckling (Fig. 12, 13). Panel pull-over and screw bending were not observed because the girt cross-section deformation dominated the failure mode. The girt cross-section was locally slender (1.52mm thick, 254mm deep), so the cross section itself deformed instead of indenting the rigid board and pulling on the fasteners (see Fig. 12). Also, the Z-section flange was too thin to develop a concentrated moment on the fastener. A secondary reason for the lack of panel pull-over failure modes is that the failure pressure for the Z250specimens was lower than that of the Z200specimens, implying that the tensile force on the screws was lower when the girts failed.

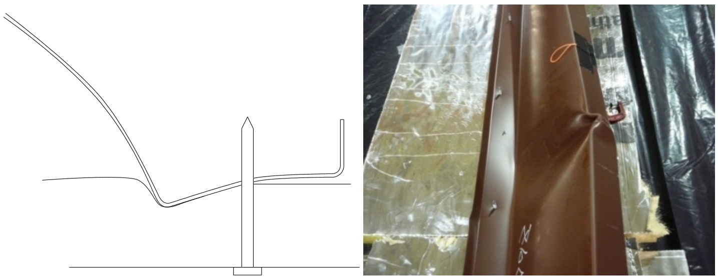

Figure 12: Deformation of slender cross section during the test

Figure 13: Local bucking during the test of slender cross section

C-section girts(203mm deep, 2.54mm thick)

It was observed that the C-section girts rotated more than the Z-section girts, primarily because of the shear center offset. This amplified rotation caused severe screw bending, because the through-fastened flange base metal thickness was thick enough (2.54 mm) to develop a concentrated moment on the fastener.

For the specimens without insulation, the failure mode was similar to the Z200 girts, i.e., panel pull-over.When 25.4mm rigid board insulation was considered, the failure mode was a combination of panel pull-over, screw bending, and fracture. Note that this result is different from the Z200 girts - no C200 specimens failed by girt yielding because the screws always broke first.

Panel pull-over was prevented when C200 specimens were constructed with 50.8mm rigid board insulation because of the “washer effect”, however the screws still bent and broke. The failure mode became more complex when the 101.6mm rigid board insulation was considered, with a combination of bent screws, broken screws, and girt yielding. The failure mode (broken screws or girt yielding) was dependent on the screw location c. The broken screw failure mode occurred in the specimens with a small c, and the failure mode of girt yielding occurred in the specimens with a larger c. This trend can be explained in Fig.14 which demonstrates that with a small c there is less pressure load (s) to prevent rotation, and therefore the screws break before girt yielding.

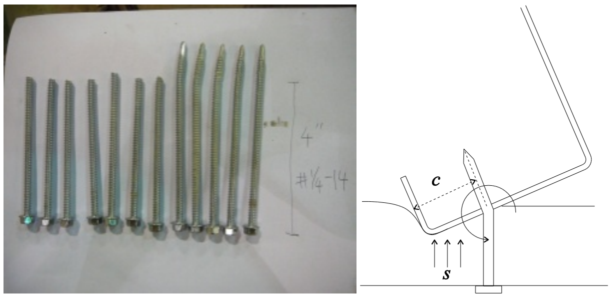

Figure 14: When *c* is small, the resisting moment is small and the screws break

C-Section (254mm deep, 1.52 mm thick)

Similar to the Z250 specimen results, all of the C250 specimens (bare panel and rigid board insulation) failed due to girt local buckling. No panel pull-over or bent/broken screws were observed.

Failure mode summary

The specimen failure modes are summarized in Table 3 as a function of rigid board thickness. All 254 mm deep members failed by girt yielding. The rigid board insulation did not influence the girt capacity because the slender (1.52mm thick) cross-section dominated the failure. For the 203 mm deep members (2.54mm thick), the failure mode changed from panel pull-over to girt yielding, the cause of which was the increased thickness of the rigid board. Thick rigid board worked like a washer, reinforcing the panel and preventing the panel pull-over. At the same time, however, the rigid board caused bent and broken screws that initiated specimen failure. The C200 girt specimens exhibited severe screw bending because of the cross-sectional twist created by the shear center offset to the applied load at the fasteners.

Table 3: Failure modes

Board Thickness	Test Name	Failure Mode
-	Z200D-1	1
	Z200D-2 Z200D-3 Z200D-R100-1 Z200D-R100-2 Z200B-1 Z200B-2W	2
25mm	Z200D-TH25-1 Z200D-TH25-2 Z200B-TH25-1 Z200B-TH25-2	2,3,4
50mm	Z200D-TH50-1 Z200D-TH50-2 Z200B-TH50-1 Z200B-TH50-2	3,4
100mm	Z200D-TH100-1 Z200D-TH100-2 Z200B-TH100-1	4

1: Panel bending
2: Screw pull-over
3: Screw broken or bent
4: Girt yielding

Board Thickness.	Test Name	Failure Mode
-	Z250D-1 Z250D-2 Z250B-1 Z250B-2	4
25mm	Z250D-TH25-1 Z250D-TH25-2 Z250B-TH25-1 Z250B-TH25-2	4
50mm	Z250D-TH50-1 Z250D-TH50-2 Z250B-TH50-1 Z250B-TH50-2	4
100mm	Z250D-TH100-1 Z250D-TH100-2 Z250B-TH100-1 Z250B-TH100-2	4

1: Panel bending
2: Screw pull-over
3: Screw broken or bent
4: Girt yielding

Board Thickness.	Test Name	Failure Mode
-	C200D-1 C200D-2	2
25mm	C200D-TH25-1 C200D-TH25-2	2,3
50mm	C200D-TH50-1 C200D-TH50-2	3
100mm	C200D-TH100-1 C200D-TH100-2	3,(4)

1: Panel bending
2: Screw pull-over
3: Screw broken or bent
4: Girt yielding

Board Thickness.	Test Name	Failure Mode
-	C250D-1 C250D-2	4
25mm	C250D-TH25-1 C250D-TH25-2	4
50mm	C250D-TH50-1 C250D-TH50-2	4
100mm	C250D-TH100-1 C250D-TH100-2	4

1: Panel bending
2: Screw pull-over
3: Screw broken or bent
4: Girt yielding

4.3 R-factors

It has been shown that the rotational restraint and the girt capacity are very sensitive to the fastener location in the flange. As *c* increases in Fig. 15 (see details in Table 2), i.e., as the fastener moves away from the cross-section pivot point on the panel, the girt capacity increases. The relationship between the girt capacity and *c* is approximately linear for a specific specimen type. However the slope of the line varies with the experimental variables, e.g., insulation thickness and cross-section type. A normalization scheme for the R-factors is implemented in the following discussion to provide a consistent comparison of girt capacity independent of fastener location.

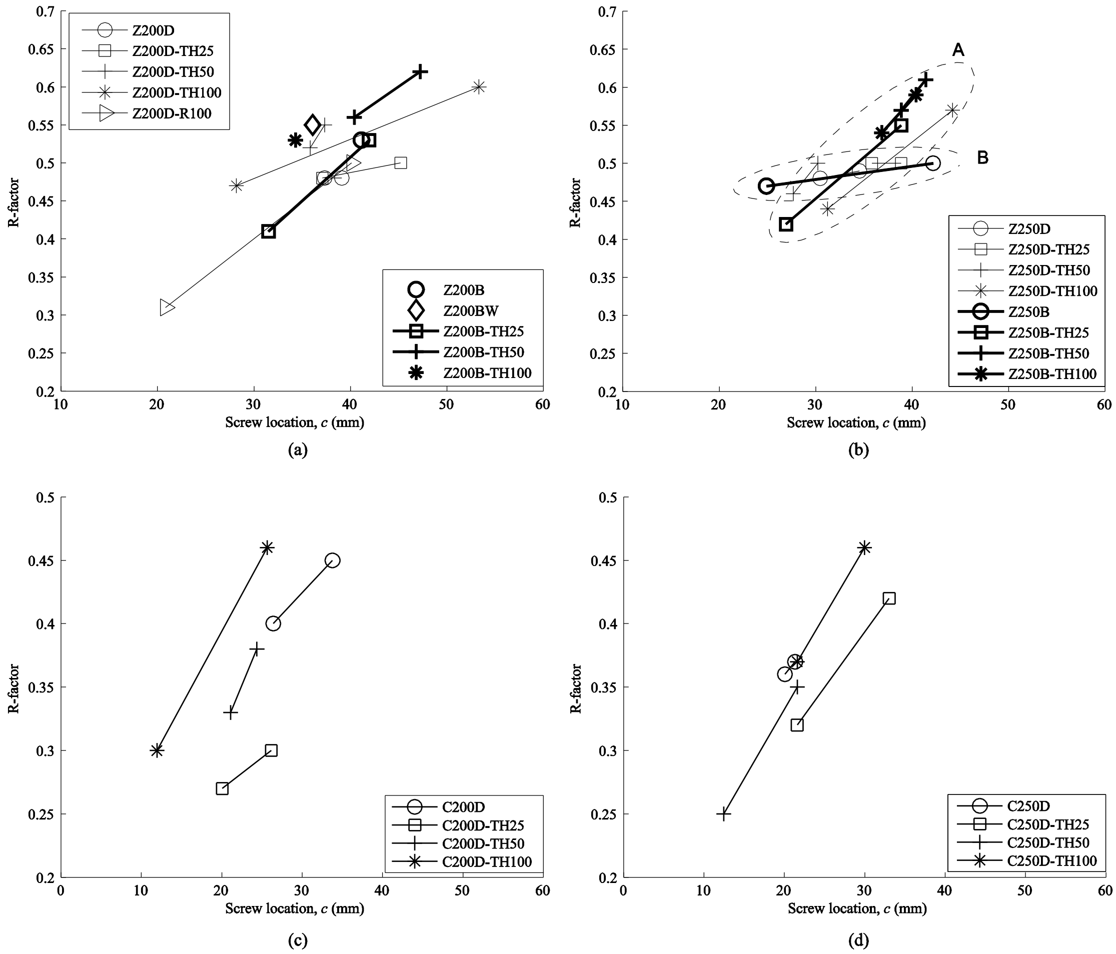

Figure 15: R-factor as a function screw location (a) Z200 (b) Z250 (c) C200 (d) C250

The current AISI prediction equations assume that the screw is placed in the middle of the flange, and therefore the R-factor is used with $c=B/2$, where B is the flange width. However, during the experiments, it was very difficult to guarantee that the screws were always placed in the middle of the flange (see Table 2),even the average c for each group (2 tests) was not assured to be close to $B/2$. To compare the results from different groups and the existing AISI S100-07 R-factors, a normalization is performed to shift all the experimentally derived R-factors in this study to $c= B/2$.

As shown in Fig. 16, two data points ([c_1, R_1], [c_2, R_2]) exist for each specimen type, and their average (c_a, R_a) can be easily calculated. The R-factor for c=B/2, $R*$, is then calculated by $R*=R_a+k(B/2-c_a)$ as illustrated in Fig. 16. The parameter k is determined in Fig. 17 by utilizing the linear relationships between the girt capacity and c for each specimen grouping in Fig. 17, i.e., for Z200, Z250 (two trend lines A and B), C200, and C250.

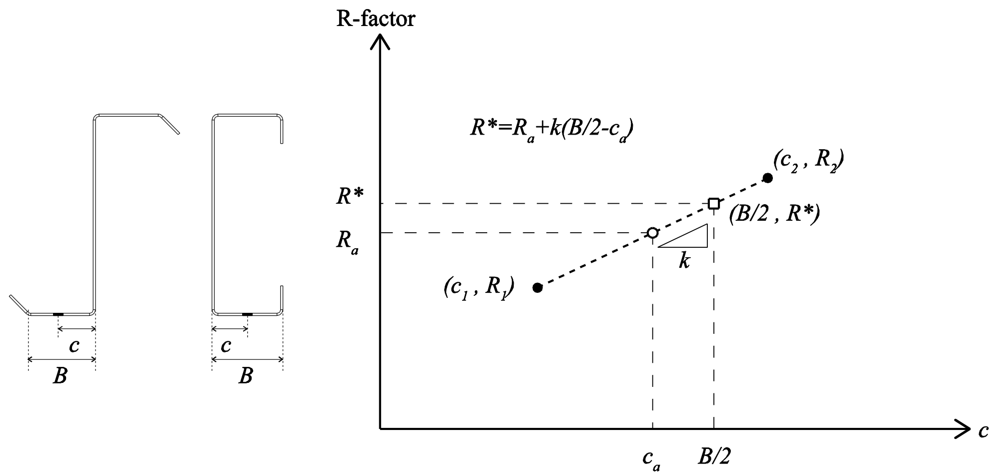

Figure 16: Illustration of correction method

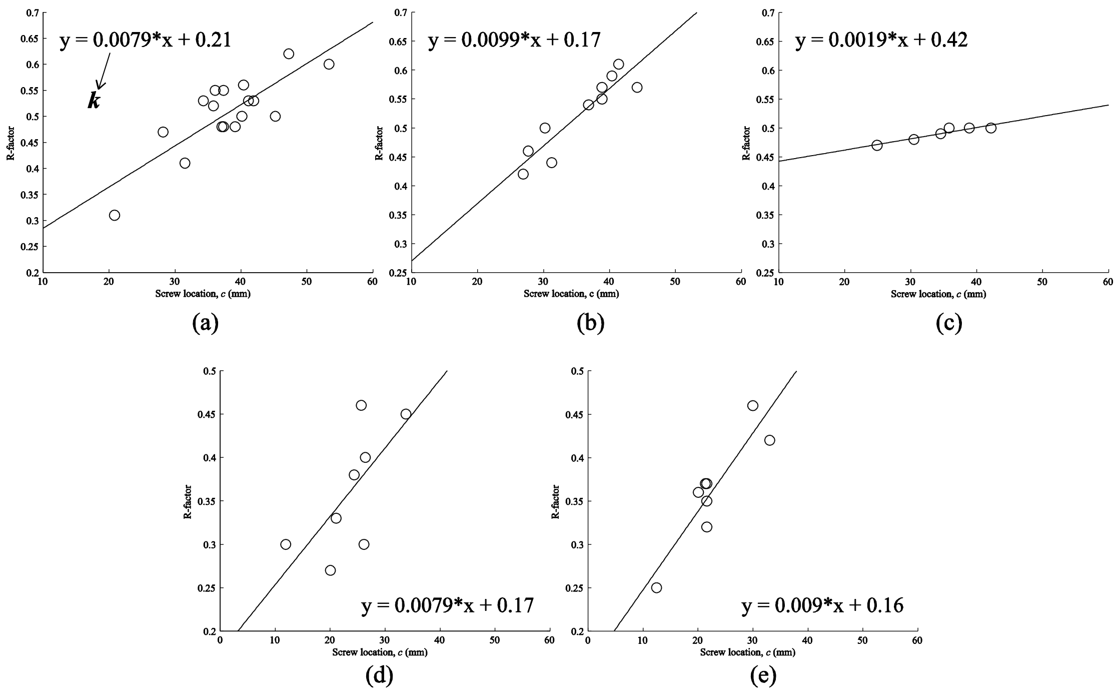

Figure 17: k-factors for (a) Z200 (b) Z250-A (c) Z250-B (d) C200 (e) C250

Bare panel trends (using Z-section)

The girt capacity trends for the Z-sections using the bare panel only are summarized in Fig. 18. (R-factors discussed in this section and in the sections to follow have been normalized for c using the procedure introduced previously.) R-factors for the Z200 girts (203mm deep, 2.54mm thick) are approximately 25% lower than the current AISI R-factor of 0.65 for 165 mm to 216 mm deep Z-sections, resulting from the panel pull-over failure mode initiated by a combination of the relatively thin 0.46mm panel and a rigid locally stocky cross-section. Adding 101.6 mm of compressible fiberglass insulation resulted in a 4% reduction in the R-factor (Z200D-R100). The R-factor for the test series Z200B is higher than Z200D, because the panel-B had a deeper rib and this panel's higher yield stress increased the panel pull-over strength. R-factor for the test series Z200BW (panel-B, fastener with washer) is higher than Z200B, because the washer improved the panel pull-over strength. Tested Z250 girt (254mm deep, 1.52mm thick) R-factors are consistent with the current AISI R-factor of 0.50. Remember, all of these locally slender members failed in local buckling. This is why the girt capacity was not sensitive to panel type (compare Z250D to Z250B in Fig. 18).

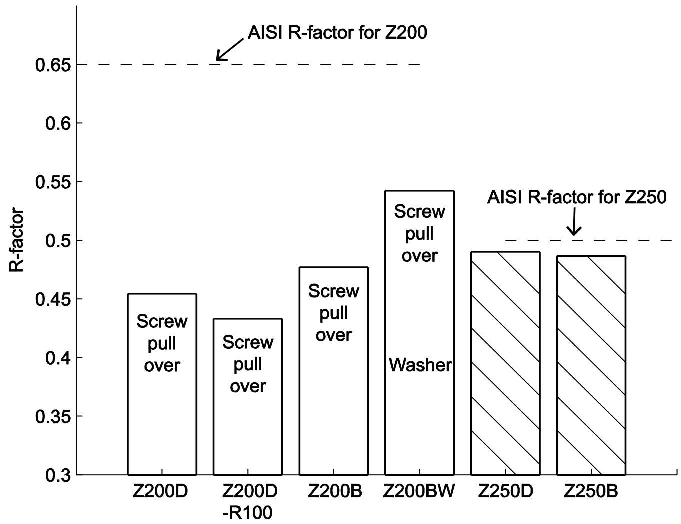

Figure 18: R-factors of the cases of bare panel

Effect of rigid board thickness (Z-sections)

The influence of the rigid board thickness on the R-factor is summarized in Fig. 19a for the Z-section's test series. For Z200girts, the R-factor of the bare panel (Panel in Fig. 19) is lower than the current AISI R-factor (0.65) because of panel pull-over. Adding 25.4mm of rigid board (TH25 in Fig. 19a) initiates screw bending and is not thick enough to provide the "washer effect" which would prevent the panel pull-over. An increase to 50.8mm of rigid board causes the failure mode to change from the panel pull-over to girt yielding, and the R-factor in TH50 increases relative to Panel and TH25. Although the failure mode for the TH50 test series is girt yielding, the R-factor is still lower than 0.65 because of screw bending and the low rotational restraint provided to the girts.

The girt capacity with 101.6mm of insulation (TH100) decreases relative to TH50, although higher rotational restraint (thicker board=higher rotational restraint) and a larger screw diameter are provided. Possible reasoning for this trend could be that the inconsistency between the principal axes and centroidal axes in the Z- section causes the cross-section to laterally shift during loading (see AISI S100-2007 commentary D3.2.1). The 101.6mm rigid board is thick enough to allow this lateral translation (the thick rigid board cannot provide a full lateral restraint). An R-factor reduction in TH100 is not observed in C-section girts where the cross section tends to rotate instead of translating laterally (Fig. 26b).

Z250 specimens consistently failed in local buckling. The test series TH25 and TH50 demonstrate a slight increase in R-factor as a function of thickness (thicker board=higher rotational restraint). This trend can be explained because the rotational restraint provided by the rigid board in the initial elastic region (see Gao and Moen 2012b) was higher than that provided by the bare panel. The decrease in capacity from TH50 to TH100 in Fig. 26a is again hypothesized to occur as an effect of the Z-section's tendency to undergo lateral translation.

Effect of rigid board thickness (C-sections)

All C200 tests (with one exception, TH100) failed because of screw failure or panel pull-over before the girts yielded. In the test series TH25, screw bending combined with panel pull-over to reduce the R-factor relative to the bare panel case. With 50.8mm of rigid board, the panel pull-over was avoided, providing higher rotational restraint than 25.4mm of rigid board and increasing the capacity (compare TH50 to TH25 in Fig. 26b). The TH100test series results in a higher R-factor than TH50 because of the improved rotational restraint from the "washer effect" as well as the larger screw diameter.

Consistent with the Z250 specimens, all C250 specimens failed in local buckling. R-factor increases slightly as a function of rigid board thickness; this is due to the aforementioned statement that the rotational restraint increases as a function of board thickness. Overall, cross-section deformation governs and the girts with a slender cross-section are relatively insensitive to the rigid board thickness.

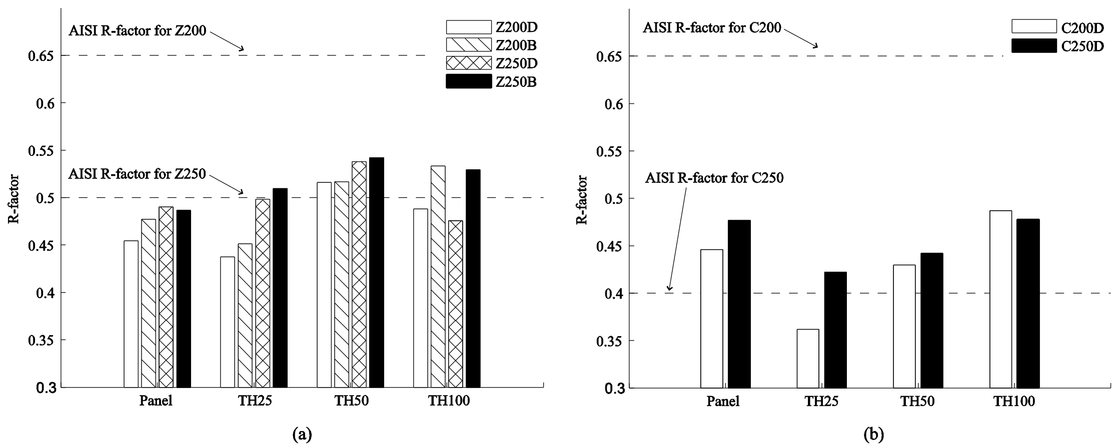

Figure 19: Influence of rigid board thickness on R-factors for (a) Z-sections and (b) C-sections

5. Conclusions

The vacuum box experiments were conducted to observe and quantify the influence of the rigid board insulation on girt capacity in metal building wall systems. The girt capacity was not influenced by the rigid board insulation when the cross-section slenderness was high (254mm deep, 1.52mm thick) because the failure mode was dominated by local buckling in the cross-section. For the locally stocky cross sections (203mm deep and 2.54mm thick), panel pull-over was observed to be the dominant limit state for tests without insulation, resulting in lower R-factors when compared to those currently specified by AISI S100-07. It is hypothesized that R-factor for Z200 girts without insulation could reach 0.65 if the panel pull-over was prevented.

Adding rigid board prevented the panel pull-over by preventing local deformation at the fasteners, i.e., the “washer effect”. However, the presence of rigid board insulation also resulted in screw bending, especially in the C-section girts, where the cross-section rotation was magnified by the torsion created because of the eccentricity of the applied load from the shear center.

References

AISI. (2007). “AISI S100-07 North American Specification for the Design of Cold-Formed Steel Structural Members.” American Iron and Steel Institute, Washington, D.C.

ASHRAE-90.1. (2010). “ASHRAE Standard: Energy Standard for Buildings Except Low-Rise Residential Buildings.” American Society of Heating, Refrigerating and Air-Conditioning Engineers, Inc., Atlanta, Georgia.

ASTM E8M. (2000). “Standard Test Methods for Tension Testing of Metallic Materials.”

AS/NZS-4600. (2005). “Australian/New Zealand Standard: Cold-formed Steel Structures.”

EN-1993-1-3. (2006). “Eurocode 3: Design of Steel Structures. European Committee for Standardization.” Brussels, Belgium.

Fisher, J.M. (1996). “Uplift Capacity of Simple Span and Zee Members with Through-Fastened Roof Panels,” *Report for Metal Building Manufacturers Association*, Cleveland, Ohio.

Gao, T., Moen, C.D. (2009). “Experimental Evaluation of a Vehicular Access Door Subjected to Hurricane Force Wind Pressures.” Virginia Tech Research Report, Blacksburg, Virginia.

Gao, T., Moen, C.D. (2011). "Flexural Strength of Exterior Metal Building Wall Assemblies with Rigid Insulation." Virginia Tech Research Report No. CE/VPI-ST-11/01, Blacksburg, Virginia.

Gao, T., Moen, C.D. (2012a). “Predicting Rotational Restraint Provided to Wall Girts and Roof Purlins by Through-Fastened Metal Panels” *Thin-Walled Structures* (accepted February 2012).

Gao, T., Moen, C.D. (2012b). “Rotational Restraint Prediction Method for Through-fastened Metal Building Wall Girts and Roof Purlins with Rigid Insulation.” *Journal of Constructional Steel Research*.

LaBoube, R.A. (1986). “Roof Panel to Purlin Connections: Rotational Restraint Factor.” *Proceedings of the IABSE Colloquium on Thin-Walled Metal Structures in Buildings,* Stockholm, Sweden.

MBMA. (2009). “Summary of Interior and Exterior Fire Wall Mock-Ups, MBMA Bulletin No. 145-09(E).” Metal Building Manufacturers Association, Cleveland, Ohio.

Murray, T., Elhouar, S. (1985) “Stability Requirements of Z-purlin Supported Conventional Metal Building Roof Systems.” *Proceedings of the Annual Structural Stability Research Council,* Cleveland, Ohio.

Pekoz, T., Soroushian, P. (1982). “Behavior of C- and Z-Purlins under Wind uplift,” *Proceedings of the Sixth International Specialty Conference on Cold-Formed Steel Structures*, November.

Rousch, C.J., Hancock, G.J. (1996). “Purlin-sheeting Connection Tests.” Research Report R724, School of Civil and Mining Engineering, The University of Sydney, Australia.

RSG. (2007). “Cold-Formed Steel Design Software.” [Computer software]. RSG Software, Inc., <http://www.rsgsoftware.com/>

Thomasson, P.O. (1988). “On the Behaviour of Cold-formed Steel Purlins-Particularly with Respect to Cross Sectional distortion.” *Baehre-Festschrift. Karlsruhe,* 281-292.

Trahair, N.S. (1993). *Flexural-torsional Buckling of Structures*. Boca Raton, Florida.

Zetlin, L.,Winter, G. (1955). “Unsymmetrical Bending of Beams with and without Lateral Bracing.” *ASCE Journal of Structural Division,* 81, 774-1.